PFC/JA-94-011

Dissipative Divertor Operation in the Alcator C-Mod Tokamak

B. Lipschultz, J. Goetz, B. LaBombard,
G.M. McCracken, J.L. Terry, M. Graf, R.S. Granetz,
D. Jablonski, C. Kurz, A. Niemczewski, J. Snipes

Plasma Fusion Center
Massachusetts Institute of Technology
Cambridge, MA 02139

June 1994

Submitted to Journal of Nuclear Materials

This work was supported by the U. S. Department of Energy Contract No. DE-AC02-78ET51013. Reproduction, translation, publication, use and disposal, in whole or in part by or for the United States government is permitted.

11th PSI Conference, Mito, Japan, May 1994

Dissipative Divertor Operation in the Alcator C-Mod Tokamak

B. Lipschultz, J. Goetz, B. LaBombard, G. M. McCracken, J. L. Terry, M. Graf, R.S. Granetz, D. Jablonski, C. Kurz, A. Niemczewski, J. Snipes
Plasma Fusion Center, Massachusetts Institute of Technology, Cambridge Ma. 02139, U.S.A.

Abstract

The achievement of large volumetric power losses (dissipation) in the Alcator C-Mod divertor region is demonstrated in two operational modes: radiative divertor and detached divertor. During radiative divertor operation, the fraction of SOL power lost by radiation is P_R/P_{SOL}~0.8 with single null plasmas, $\bar{n}_e$ < $2x10^{20}$ m^{-3} and I_p< 1 MA. These plasmas sometimes have very high recycling, with $n_{e,div} \leq 6 \times 10^{20}$ m^{-3}.

As the divertor radiation and density increase, the plasma eventually detaches abruptly from the divertor plates: I_{SAT} drops at the target and the divertor radiation peak moves to the x-point region. Probe measurements at the divertor plate show that the transition occurs when T_e ~ 5 eV. The critical $\bar{n}_e$ for detachment depends linearly on the input power. This abrupt divertor detachment is preceded by a comparatively long period (~1-200 ms) where a partial detachment is observed to grow at the outer divertor plate.

I. Introduction

Owing to the impetus of the ITER EDA [1], there is increased interest in maximizing the dissipative nature of the divertor through volumetric power

losses. An important specification of the current ITER design is that the peak heat load on the divertor plates must be within tolerable engineering limits (~ $5MW/m^2$). Given the large SOL power flows predicted for ITER, a physics solution that reduces the heat loads must be found. Research has thus focused on obtaining a 'dissipative' mode of operation whereby the power flowing into the divertor region is distributed by radiation and CX neutrals over large areas of the divertor.

Assuming that dissipative divertor operation can be obtained, it is important to determine whether this operating mode can be sustained in cases where the parallel heat flow in the SOL (in C-Mod presently ~ $200\ MW/m^2$) is comparable to that expected in ITER (500 - $1000\ MW/m^2$) while at the same time keeping the central plasma free of imputities.

Initially, the search for a ITER divertor solution has concentrated primarily on enhancing the divertor radiation. Utilizing radiation to remove more than ~50% of the power flow to the divertor may be difficult [2]. However, it is recognized that if parallel momentum is removed from the plasma flowing to the target, increasing amounts of radiated power may be more readily achieved. Stangeby [3] has shown that the required momentum loss might be achieved through charge-exchange and elastic ion-neutral collisions. If large enough, these momentum losses can lead to plasma detachment from the divertor plates.

The divertor geometry and density range of Alcator C-Mod are significantly different from other existing tokamaks. These differences should enhance the dissipative capabilities of the C-Mod divertor. The geometry and high density allow better trapping of neutrals in the divertor. The high density also enhances dissipative processes (radiation, CX and ion-neutral collisions) which are

proportional to n_e.

Two general types of dissipative divertor characteristics have been observed in Alcator C-Mod; a 'radiative' divertor and a 'detached' divertor. The definition for radiative divertor in Alcator C-Mod is that $P_{rad,div}$ be large (i.e. > .25 × P_{SOL}, $P_{SOL} = P_{IN} - P_{rad,main}$) and that pressure be approximately constant along a flux surface. Detached divertor operation is defined to be when pressure is no longer constant along flux tubes which connect to the divertor surface. This process typically is manifested as a drop in I_{SAT} at the plate.

II. Tokamak Description

Alcator C-Mod is a single-null divertor tokamak. The high-field capability, combined with small major radius, allow very high central plasma densities and plasma currents. The first-wall material is molybdenum. Table 1 lists present and design parameters for the Alcator C-Mod device. Further details of the machine design and operation can be found elsewhere [4,5,6,7]. Initial experiments focused on developing methods of controlling the plasma position and shape and optimizing equilibria for divertor operation. The vessel is conditioned by a vacuum bake to 150^{0}C and by Electron Cyclotron Discharge Cleaning.[7]

The lower divertor geometry (see figure 1) can be characterized as comparatively closed with the minimum opening determined by the points of closest distance to the x-point (herein called the 'nose' of each divertor plate). The divertor plates are shaped such that they function both as divertor plates and baffles. Below the divertor noses, the orientation of each plate is such that recycling neutrals primarily leave the surface with trajectories away from the central plasma.

This is in contrast to standard, more open divertors. A second consequence of the angle of the divertor plate is that these neutrals are launched towards the local separatrix. This effect is expected to increase recycling (density) on the separatrix and lower the temperature there.

The divertor and edge regions have been studied with bolometer arrays, visible spectroscopy and Langmuir probes. There are 48 Langmuir probes located in the divertor plates consisting of 16 sets of three probes (triplets), 10 on the outer divertor and 6 on the inner, fig 2 [8]. The probes of a given triplet are located at the same poloidal position, separated toroidally by 6 m m. 5 of the 48 probes project above the divertor surface (so-called 'domed' probes) and are used to obtain local density and temperature. The remaining 43 probes have surfaces that are 'flush' with the divertor surface and are utilized only for qualitative measurements of ion-saturation currents (I_{SAT}) because of the nonlinear increase in collection efficiency at low field-line incidence angles [9]. For reference, the triplets of probes are numbered in figure 2; domed probes have a 'D' beside the probe location. In this paper the probes will be referred to as OD-1 through OD-10 on the outer divertor and ID-1 through ID-6 on the inner divertor. The SOL is diagnosed with a single Langmuir probe, which can be pneumatically scanned through the edge plasma (see figure 2) [8]. Together, the SOL and divertor Langmuir probes provide the available edge density and temperature measurements. By convention, the density information from these probes will be presented as n_∞, the equivalent density far from the sheath.

A crucial measure of the efficacy of power dissipation in the divertor is the power lost in that region before being conducted to the plates. Two bolometer

arrays, labeled in figure 3 as B1 through B8, have views across the divertor x-point region. These bolometers [10] measure the total radiation and neutral particle losses from the divertor region. A third array of detectors, labeled UV-1 through UV-16, consists of UV-enhanced diodes which have a view of the divertor region from below (figure 3). This array is primarily used for locating the radiating region. The power loss from the main plasma is measured with a 24-channel, toroidally viewing bolometer array [10].

Spectroscopic information is collected from several sources. Light emitted from the outer divertor was imaged into a spectrograph which has an OMA detector [11]. This system has a spectral coverage of 200-750 nm and has been utilized to determine both impurity source rates and local electron densities by observation of Stark broadening. Filtered diode arrays with over 200 chordal views were also utilized for visible light emission measurements [12-14]. The filters can be changed to allow measurement of H_α and C-III brightness profiles in the main chamber and the divertor. Figure 4 provides a layout of these arrays and the OMA views. The brightness information from these measurements can been inverted to obtain emissivity distributions utilizing a numerical technique described elsewhere [13].

III. Radiative divertor

The standard operation of Alcator C-Mod results in a highly-radiative divertor; a large fraction of the power flowing to the divertor ($\sim .8 \times P_{SOL}$) being removed from the plasma before reaching the divertor plates. Figure 5 illustrates the dependence of the total power removed from the plasma as measured by the bolometer arrays (radiation + charge-exchange). The input power and plasma

current variation included in this data are 0.4 - 2.0 MW and 0.4 - 1.0 MA respectively. These data were obtained during discharges without addition of extrinsic impurities.

III.1 Radiation

Carbon and oxygen radiation play a more important role in the divertor power balance. The OMA spectrograph has been used to characterize the dominant impurity source rates from the outer divertor. The carbon and oxygen source rates are determined by monitoring the emission lines at 426.7 (C-III) and 435.1 nm (O-II) respectively and are typically in the ratio of ~3:1. This ratio of fluxes is comparable to measured impurity influxes from the surface of the inner wall limiter. In the divertor, the molybdenum source rate from the target tiles is usually negligible [14]. From the diode arrays the C-III emissivities are found. An estimate of the total carbon emission has been made using the 1-D impurity transport code MIST [15], based on local C-III emissivity together with probe measurements of n_e and T_e [10]. Carbon radiation appears to be a major contributor to the divertor radiated power. The emissivity distribution of oxygen emission has not been directly measured but assumed to be similar to carbon with magnitude reduced by a factor of ~3 due to differences in the measured source rates. Hydrogen is not an important contributor to the divertor radiation.

Although a mathematical inversion of the bolometer data has yet to be accomplished, the brightness data show that the majority of the divertor radiation is peaked along the outer divertor separatrix leg, from the x-point region to the strike point. In general the emissivity distribution for carbon correlates with the

bolometry information and does not vary significantly over the range of operation (except when a transition to detached divertor occurs).

III.2 Divertor plasma parameters

An important function of divertor radiation is that it helps reduce the divertor plate plasma temperature, leading to an increase in the density there. Figure 6 shows the scaling of the density at the outer divertor domed probe location OD-7 (see diagnostics figure). Referenced to the midplane, the probe data shown maps to approximately 1-2 mm outside of the separatrix (λ_n ~ 10 mm). The divertor density increases approximately linearly with $\bar{n}_e$ at low densities. At high densities the dependence of $n_{e,div}$ on $\bar{n}_e$ becomes very nonlinear; a 'high-recycling' divertor. The data set obtained at different plasma currents are offset (in $\bar{n}_e$). This offset is removed by plotting the data vs. $\bar{n}_e/I_p$ [8]. Although $n_{e,div}$ can be significantly higher than $n_{e,sep}$, pressure is still approximately constant along a flux surface.

IV. Detached Divertor Operation

IV.1 General characteristics

Although radiative divertor operation removes the majority of the power flowing to the target plates, even more dissipation of the divertor power flow may be required for ITER [16]. Recently, in a number of divertor experiments [17-19], an approximation of this ideal has been achieved; the so-called 'detached divertor', where there is a strong gradient in pressure from the SOL to the divertor plates. These detached divertor conditions have also been observed in Alcator C-Mod. As

$\bar{n}_e$ is increased (or plasma current decreased) an abrupt transition from standard radiative divertor to detached divertor occurs. An example of the effect on the outer divertor is shown in figure 7. The plasma current is constant with the central density rising when, at 0.725 seconds, the ion saturation currents on the outer divertor probes exhibit a rapid change or rearrangement. The separatrix strike point is between probes OD-5 and OD-6. At probes OD -1 through OD-7, which are located below the nose of the outer divertor, I_{SAT} drops. The opposite is true at probe locations at and above the nose. This effect is quite similar and occurs simultaneously at the inner divertor; I_{SAT} drops for all probes below the nose (ID-1 through ID-4) with corresponding increase in I_{SAT} above the nose (ID-5 and ID-6). The main difference between the inner and outer divertor is that the probe located at the nose on the inner divertor (ID-4) almost always exhibits a drop in I_{SAT} while the probe located at the nose of the outer divertor (OD-8) almost always stays constant or slightly increases.

There are a number of other characteristics, both in the edge and central plasmas that are affected by the transition to detached divertor operation. Figure 8 includes waveforms of a number of plasma characteristics for the same shot as shown in figure 7. At detachment, the time-derivative of $\bar{n}_e$ increases without a change in gas-puff rate. A similar effect is often observed in the behavior of the midplane neutral pressure measurement. The absolute magnitude of the divertor radiation does not change significantly although its spatial distribution does. For the purpose of power accounting, any radiation measured by the divertor bolometer arrays is considered 'divertor' radiation. This is true even though one chord (B1) views above the x-point and thus through a section of the main plasma. The

central plasma radiated power does not exhibit any abrupt change in magnitude. There is a change in rate of increase following detachment. This leads to higher central radiated powers [10].

The domed Langmuir probes allow determination of the evolution of density, temperature and pressure through the period of detachment, figure 8. The time resolution of this data is limited to 10 ms (the sweep period of the Langmuir trace). Using the flux surface information obtained from EFIT [4,5,20], all divertor probe locations are mapped back to the plasma midplane, ρ_{mid}, the distance outside the separatrix. In the period approaching detachment, n_e at probe OD-7 increases nonlinearly with $\bar{n}_e$ as the corresponding T_e decreases in a manner that keeps the parallel heat flux approximately constant. Comparison of this data to the corresponding SOL probe measurements on the same flux surface shows that pressure is approximately constant along a flux surface. Just prior to detachment, the local electron temperature near the outer divertor nose (probe OD-7) for this shot, and for all data examined, is close to 5 eV (~4 - 7 eV). After detachment, the density at the detached location is low, typically around 2-5 $\times$ $10^{19}m^{-3}$ while T_e remains at ~ 5 eV.

Further out in the common flux region, the situation at the divertor surface is considerably different. Again, referring to figure 8, the density at probe OD-9 increases nonlinearly with $\bar{n}_e$ in the period before detachment and T_e decreases (though not with as strong a dependence as seen on probe OD-7). During this period there is often a lower T_e at points closer to the separatrix (e.g. probe OD-7) than at OD-9. At detachment, the density at probe OD-9 abruptly increases. The

corresponding T_e continues to fall (staying $\geq$ 5 eV) as the local density increases.

Significant changes in the SOL density and temperature profiles are also seen at detachment. $n_{e,sep}$, λ_n and λ_T can all increase substantially while $T_{e,sep}$ drops. These observed changes are consistent with the increase in $\bar{n}_e$ after detachment [8].

The SOL and outer divertor probe data can be compared, at the same ρ_{mid}, to determine the effect of detachment on pressure. After detachment, at regions of the divertor plate which are detached (e.g. probe OD-7) pressure is lower than in the SOL. For non-detached regions above the divertor nose (e.g. near probe OD-9), pressure is still constant on a flux surface.

IV.2. Processes leading up to detachment

The abrupt changes in the divertor that occur at divertor detachment are often preceded by a slow process, lasting 100-200 ms, of a more localized detachment along the outer divertor surface. This behavior is illustrated in figure 9. For this data, the separatrix is located in the region between probes OD-3 and OD-4 and is constant, within $\Delta\rho_{mid} \sim 1$ mm over the 200 ms before detachment. Even so, one can see that the I_{SAT} profile peak moves up the divertor plate towards the nose (0.35 to 0.67 s) and away from the separatrix. The I_{SAT} peak reaches probe OD-7 (just below the nose) at the time when overall divertor detachment occurs. This localized detachment effect is not found at the inner divertor.

After the I_{SAT} peak passes a point on the divertor plate, the plasma in the connecting flux tube detaches. Examining the domed probe data in figure 9 (OD-3, near the separatrix) n_e drops (T_e is already $\sim$ 5 eV) while the general SOL is unaffected. After examination of a number of shots where this has occurred, three

points are noted: (1) Constant pressure along a flux surface does not hold (definition of detachment) at locations where the peak has passed; (2) localized detachment appears to start in the private flux region and; (3) When the peaking reaches the region of probe OD-7 overall divertor detachment occurs. The plasma, through this local detachment process, is slowly 'unzipping' from the outer divertor plate. This 'unzipping' process occurs even in Alcator C-Mod discharges that do not reach the stage of overall detachment; i.e. the density peak does not reach the outer divertor nose. This localized detachment could be interpreted as a steady state detachment with radiation and pressure gradient along a flux surfaces, a thermal front [21], located well inside the divertor. For the remainder of this paper the process described above will be referred to as 'localized' detachment as opposed to the more general abrupt divertor detachment that follows it.

An obvious question is whether the observed movement of the density peak relative to the separatrix is really due to a time-dependent inaccuracy in the magnetics. Comparison of the separatrix location obtained from the density peak to that from the magnetics in non-detached discharges leads to a conclusion that there may be a systematic offset in the separatrix location (~ ± 1 mm) but not a time-dependent error.

There is movement of the divertor radiation emissivity peak which is correlated with the probe data. Figure 9 includes brightness data from chords UVB13-16 of the UV bolometer array (see figure 3 for geometry) for comparison with the probe I_{SAT} data. The movement in the drop of I_{SAT} up the divertor plate correlates with a similar movement of the reduction in UV bolometer chord brightness. The abrupt total divertor detachment can be seen at 0.675 sec when

there is a decrease in radiation at all UV diode chords. UV-16 does not decrease prior to divertor detachment due to chordal integration along most of the separatrix leg.

IV.3 Effect of divertor geometry

The effect of divertor geometry on detachment, as well as the preceeding localized 'unzipping', are important factors in the understanding of divertor physics and in future divertor designs. During this run period the variations in Alcator C-Mod geometry have been limited to placement of the separatrix strike point at different locations on the outer divertor. The limits of this placement for which data is available are between probes OD-2 and OD-7. The principal characteristics of the detachment process are unaffected by the separatrix location: Detachment is limited to regions below the outer divertor nose and T_e at probe OD-7 (just below the nose) is always ~ 5 eV. The closer the separatrix is located to the outer divertor nose the shorter the period of localized detachment before overall divertor detachment.

IV.4 Detachment scaling

The threshold for full divertor detachment in Alcator C-Mod operational space for ohmic plasmas is reproducible. Figure 10 displays the relationship between the $\bar{n}_e$ detachment threshold and input power for both ohmic and RF-heated discharges. For ohmic plasmas the dependence is linear over a wide range of plasma currents (0.4MA - 0.85 MA). Higher current discharges have been obtained,

but the plasma density has been less than the threshold $\bar{n}_e$ predicted on the basis of this figure. Note that the threshold for detachment is at a small fraction (~25%) of the density limit [22] for ohmic plasmas. The difference between the scaling of the detachment threshold for ohmic and RF-heated plasmas is striking. Assuming that all the forward RF power is absorbed in the plasma core there is considerably higher input power for a given threshold $\bar{n}_e$ than for ohmic plasmas. If one assumes that $T_{e,div}$ is a necessary condition for detachment then examination of simple 2-point analytic models for the SOL [2,3,8] leads to a conclusion that P_{SOL} and P_{DIV} are the more important factors determining detachment, rather than P_{IN}. The ohmic and RF data correlate if account is taken for the radiation in the divertor and core plasmas, i.e. P_{IN} is replaced by P_{DIV}. In general this is found to be true. Unfortunately, the uncertainties in all the variables is large.

IV.5. Neutral density

Neutrals play an important role in current models for the physics of detachment. Because of the significant role these neutrals can have, the neutral atom density in different regions of the SOL and divertor have been studied. First, let us examine the atomic neutral density in the SOL. Equating molecular flux ($\frac{1}{2} n_{om} \bar{v}_m$) outside the SOL to the atomic flux with Franck-Condon energy ($n_{oa} v_{fc}$) in the plasma the equivalent atomic density at the edge of the SOL, can be derived from the molecular D_2 pressure at the midplane, figure 11. These data do not represent the neutral density near the divertor surface.

Two methods have been used to investigate the neutral density at the

recycling surfaces. The first method involves experimental H_α chordal brightness (recycling light) and Langmuir probe measurements at the same outer divertor surface location. The neutral density is derived from the following equation:

$$B(H_\alpha) = \int d\ell \; (n_0 n_e \langle \sigma v \rangle_{ex}) \sim \Delta\ell \; (n_0 n_e \langle \sigma v \rangle_{ex})$$

Knowledge of T_e and n_e from the local probe are utilized. $\langle \sigma v \rangle_{ex}$ is the electron excitation rate for H_α.

The second method calculates the penetration of the Franck-Condon neutral atoms into the SOL plasma based on a Monte-Carlo technique, the real divertor geometry and experimentally derived n_e and T_e profiles. Given the assumption that the neutral flux leaving the surface is equal to the incident ion flux, $\frac{1}{2} n_e c_s \sin\theta$ (θ is the field line incidence angle), a neutral density profile can be determined (neglecting ion-neutral processes).

These two methods have been compared with respect to the number of H_α photons generated per atom launched (a typical value is .03 H_α photons/atom). The methods roughly agree for non-detached divertor plasmas (within a factor of 2) if the energy of the neutrals launched from the divertor surface is assumed to be ~ 2 eV (Franck-Condon neutrals produced by dissociation).

The neutral densities at the divertor plate surface for non-detached divertor plasmas inferred by the above methods at probe location OD-7 are significantly higher than at the SOL, figure 11. The corresponding mean free path for ions flowing along a field line colliding with neutrals (elastic or CX) varies from ~.1 to 1 m over the range of data shown. Since the connection length from the divertor

plate back to the x-point region is of order 2-3 meters, ion-neutral collisions are probably removing a significant fraction of the ion momentum even for non-detached divertor plasmas.

Utilizing the neutral density profile in the SOL calculated above, an estimate of the local charge-exchange rate (and ion-neutral elastic collision rate) was made. This is an overestimate of the local rates because the ionisation and charge-exchange are competing processes and multiple generations are not taken into account. The volume power loss rate found ($\sim 1 \times 10^7$ MW/m^2) at the highest densities before detachment is of the same order as that determined from the divertor bolometer chords and estimated from the C emission measurements. Thus neutral-related loss processes are significant in the divertor power balance as well as playing a role in momentum losses.

IV.5 Radiation

As discussed in section III, the divertor radiation is typically $\geq 0.8 \times P_{SOL}$. Prior to detachment, the radiation is peaked along the separatrix outer divertor leg. At detachment there is a rearrangement of the radiation with the peak in the emission moving up above the x-point. Figure 12 shows a C-III emissivity contour plot of the divertor region after detachment. This figure is obtained by an inversion of the~ 120 CIII-filtered diode array chords available for this shot [13]. A significant fraction of the C-III emission moves inside the separatrix after detachment. For comparison, the divertor bolometer arrays also indicate that the peak in total emissivity moves up to the x-point and above, after divertor detachment. This movement can be slow (10's of ms) compared to the drop in I_{SAT} at the divertor

surfaces.

IV.6 Core Plasma Transport

The onset of detachment can also have significant effects on the impurity level in the plasma. Trace impurity injection [23] shows that the global impurity particle confinement time for scandium is unaffected by the transition from radiative to detached divertor. To determine the effect of detachment on central impurity densities, emissions from H-like C (2p-1s; 33.74 Å), He-like C (2p1s - $1s^2$; 40.7 Å) and He-like Ar (2p1s - $1s^2$; 3.949 Å) have been monitored through the period of transition to detached divertor. It is found that the levels of these impurities in the central plasma increase by a factor of ~ 2 after detachment. MIST has been employed [23,24] to model the central impurity transport using measured SOL profiles and the transport coefficients determined from the trace impurity injection. The observed changes in carbon and Ar levels in the plasma can be reproduced with the model by including the observed changes in the SOL density and temperature profiles with no need to increase the impurity source rates at the walls or in the divertor. This result is consistent with the observation that neither the rate of Ar injection nor of the CIII-derived source change at divertor detachment.

The effect of detachment on deuterium transport is less clear. While the total density in the central plasma rises after detachment, the total H_α emission from around the chamber does not vary significantly, τ_p increases by ~ 20%. However, comparison of the relative magnitude of the 8 density interferometer chords through the period indicates no significant change in the density profile shape and thus transport.

V. Discussion

V.1 Radiative divertor

The radiation and recycling characteristics of the radiative divertor are consistent with a simple 2-point analytic model of the edge and divertor plasma [25]. Considering this model together with a simple estimate of the SOL thickness [26], the variations of divertor parameters can be reasonably reproduced. Boundary conditions used are the input power, $\bar{n}_e$, a $\chi_\perp$ consistent with the radial temperature gradient in the SOL and radiation losses (divertor and central plasma). The results of this model are shown in figure 13 along with divertor data for two plasma currents (~600 and ~ 800 kA). The change in slope seen at $\bar{n}_e \sim 1 \times 10^{20}$ m^{-3} is due to a change in parallel heat flow regimes. At low $\bar{n}_e$ collisionality is low and parallel heat flow is limited by the conduction through the sheath. As the density increases, a transition is made from sheath-limited parallel flow to the standard Braginskii parallel conduction of heat through collisions; the conduction-dominated regime. The level of radiation in the Alcator C-Mod divertor is an important factor in the application of this model. Without radiation the power density in the SOL would be higher and the transition to the conduction limit would occur at higher $\bar{n}_e$. A more in-depth treatment of SOL transport scaling based on interpretation of the C-Mod data is presented in a companion paper by LaBombard[8].

V.2 Detached divertor

V.2.1 General characteristics

The characteristics of general divertor detachment observed in Alcator C-Mod are consistent with the model proposed by Stangeby [3]. T_e in the region of local detachment (or total detachment) is always ~ 5 eV, allowing charge-exchange and elastic ion-neutral collisions to dominate over ionization in processes involving neutrals. The neutrals can then acquire a significant fraction of the ion momentum and exit the divertor fan without ionization.

Hutchinson, using a 1-D model [21], has studied the stability of thermal fronts. That model shows that if the radiation profile along a flux surface is fairly uniform, the detachment location can gradually move from the divertor plate to the x-point as $\bar{n}_e$ is increased. The density range predicted by that model over which this stable detachment would occur was about 20% of $\bar{n}_e$. The behavior exhibited by local detachment is consistent with that prediction; as $\bar{n}_e$ is increased the localized detachment moves up the divertor face. When general divertor detachment occurs, the changes in divertor profiles are faster than localized detachment. This leads one to suspect that a very unstable process is involved. The different time-dependence of localized and divertor detachment imply that the 2-D nature of the problem must be taken into account.

V.2.2 Local detachment process

The general divertor detachment, determined by the drop in I_{SAT} on all probes below the divertor (inner and outer) noses, is preceded by a slow, local detachment moving across the outer divertor plate. This local detachment, the characteristics of which are explored in section IV.2, starts in the private flux region, moves across the separatrix and the common flux until just below the nose. At that

point the general divertor detachment ensues. The form of this local detachment can be pictured as a 'front' (figure 14). The density drops along a flux surface from the front to the plate. Above the front, the plasma characteristics are relatively unaffected.

Localized detachment on one flux surface, in turn, could influence detachment on the neighboring flux surface. When a flux surface locally detaches from the plate, the observed particle flux to the divertor plate decreases. However, the ionization above the front, on the same flux surface, is probably not significantly changed. Ionization of recycled neutrals from attached flux surfaces (see n_0 in figure 14) as well as particle flow from the SOL will cause a continuous flow of ions towards the front. Those particles could diffuse outward to the next flux surface that is still 'attached' to the target plate. The particle flux to the plate is thus increased on the attached flux surface and with it the local n_e (with a corresponding decrease in T_e) bringing that location closer to detachment. As this process repeats itself, localized detachment could push a density peak ahead of it as it proceeds through the common flux region. Moving away from the separatrix, the density, power flow and ionization source that are feeding into the attached flux surface all decrease. As a result the density peak should decrease as well. This picture appears to be consistent with the behaviour as the localized detachment approaches the region of probe OD-7 (figure 9).

V.2.3 Causes determining the extent of general divertor detachment

Aspects of magnetic geometry also do not appear to correlate with the spatial extent of detachment. As the strike point location is varied over the outer divertor

face, the physical extent of detachment (the nose) does not correspondingly change. Because the spatial limit of detachment on the outer divertor is located between probes OD-7 (detaching) and OD-8 (non-detaching), one asks whether there is a strong variation in any magnetics quantity across that region. Neither connection length (to the x-point region or to the midplane) nor field line angle vary strongly between those two locations. It thus seems unlikely that magnetics alone determine the spatial extent of detachment. Likewise, there is not a significant difference between probe OD-8 and OD-7 with respect to the proximity to the x-point and a perceived source of heat. This is especially true if one compares the location of those probes to ID-4 (detaches) on the inner divertor. That location is much closer to the x-point.

There is a significant difference between the effect of recycling at probes OD-7 and OD-8. The former is located such that recycled neutrals are aimed towards the outer leg of the separatrix. Those neutrals are more likely to cause additional ionization and density increase just above the ionization front. This could accelerate detachment. At the latter probe, OD-8, recycled neutrals are launched more towards the x-point and the SOL. Those neutrals will be spread over a larger range of flux surfaces thus diluting their local effect.

In summary the reasons for the extent of general detachment always being limited to below the nose are not clear. There is evidence that the magnetic geometry alone (e.g. field line angle, connection length and proximity to the x-point) is not the cause. Recycling characteristics (dependent on physical geometry) could play a role but there is no strong evidence to support this conjecture. The strongest evidence against magnetics-related causes (and for geometry) is that the

location of the strike point at different points along the outer divertor face does not affect the detachment extent along the divertor face. The question is further confused by the experimental results from DIII-D [18] and JET [17]. In both of those tokamaks the geometry is open and flat; very different from that of C-Mod. However, the extent of detachment is reported to be different in those two experiments; complete SOL in JET, partial in DIII-D.

V.2.4 Implications of these results

What are the implications for future tokamaks? The radiative divertor, in it's C-Mod manifestation, is useful in dissipating most of the input power (> 80% of the power flowing into the SOL). A number of the aspects of detached divertor operation observed in Alcator C-Mod may be advantageous for ITER. When general divertor detachment occurs, the power conducted to the plates is reduced below even the low levels of the radiative divertor. The ionization region shifts away from the plates along withthe peak in the radiation emissivity to inside the separatrix; power is well spread over the surrounding surfaces. The location of the radiating region outside the divertor, much less above the x-point, negates the purpose of allocating large parts of the vessel volume to divertor hardware.

There is an additional potential problem for ITER predicted by C-Mod results. The general detachment threshold for Alcator C-Mod ohmic plasmas occurs at ~ .25 × the Greenwald density limit. ITER operation is predicated on operating at or above the same limit. The relationship between detachment threshold and density limit is therefore of great importance. The difference between $n_{detach}/\bar{n}_{limit}$ in C-Mod and other experiments could be due to a number of factors; divertor geometry,

heating methods, first-wall material, size etc..

The process of localized detachment from the divertor plate may be more attractive than general divertor detachment. Apparently, the density is reduced at the divertor plate and the radiation shifts away as well. A steady state localized detachment could combine the best of radiative and detached divertor characteristics.

VI. Summary

The amount of radiation in the divertor region of Alcator C-Mod is significant in reducing the power flow to the divertor plates. Radiation from this region is consistently of order or larger than that of the central plasma. On the basis of experimental measurements and modeling it is estimated that hydrogen charge-exchange and carbon line emission account for most of these power losses.

The radiative divertor operation can be divided into two transport regimes; sheath-limited and conduction limited parallel heat flow. In the former regime, density and temperature are approximately constant along a flux surface and divertor parameters are linearly dependent on SOL values. As $\bar{n}_e$ increases, or input power decreases, conduction-limited flow is achieved. In this regime the divertor parameters are nonlinearly dependent on the SOL characteristics.

The characteristics of divertor detachment in Alcator C-Mod have been determined. Just prior to detachment $T_{e,div}$ in the regions below the divertor nose is ~ 5 eV. Radiation in the divertor is high such that $P_{DIV} \sim .8 \times P_{SOL}$. Local detachment is occurring along the outer divertor plate surface, 'unzipping' the plasma off of the plate towards the divertor nose. The SOL characteristics away

from the divertor are unaffected.

At the point where the local detachment process reaches the region of the divertor nose (OD-7) general divertor detachment occurs. This is much faster than the local detachment and affects all locations on both divertor plates. On the surface of the divertor plates, below the nose, the density drops abruptly. Above the divertor nose, farther out into the SOL, the density increases. The peak in the radiation emission shifts to the x-point and above.

Due to the changes in the SOL, impurities and hydrogenic species can more easily penetrate across the separatrix. The transport of impurities and hydrogenic species in the core of the central plasma does not change after detachment and thus both the electron and impurity densities increase.

Input power, radiation and $\bar{n}_e$ all play an important role in determining the transition to divertor detachment. As the power flowing into the divertor is reduced (radiation increased), or $\bar{n}_e$ increased, $T_{e,div}$ is decreased until 5 eV is reached and divertor detachment ensues. It is important to note that this behaviour occurs at densities much below (~25%) the Greenwald limit.

Acknowledgements

The authors would like to extend appreciation to Professors I. Hutchinson and P. Stangeby for very helpful discussions. The Alcator group has supplied very important support in many ways. In particular, Dr's Steven Wolfe and Steven Horne have provided an invaluable service in bringing the plasma control to a mature level such that the diverted plasmas required for this study could be produced. This work was supported by U.S. D.oE. contract # DE-AC02-78ET51013.

References

[1] Details of the ITER Design Report, 4th Meeting of the Technical Advisory Committee, San Diego Joint Work Site, 10-12 January 1994.

[2] G M McCracken and Pedgley, Plasma Physics and Cont. Fusion, 35 (1993) 253

[3] P C Stangeby Nuclear Fusion, 33 (1993) 1695

[4] I Hutchinson, R Boivin, P Bonoli et al MIT Report PFC/CP-93-1, See National Technical Information Service document no. DE94001565.

[5] I H Hutchinson, R Boivin, F Bombarda, Physics of Plasmas, 1 (1994) 1511

[6] B Lipschultz J Goetz, B Labombard and G M McCracken, this conference

[7] E L Marmar, C Christensen, J Goetz et al, Bull Amer Phys Soc 38(10) 1993, paper 3S18, pg 1956.

[8] B Labombard, D Jablonski, B Lipschultz, et al, this conference.

[9] G F Matthews, S J Fielding, G M McCracken et al, Plasma Physics and Controlled Fusion 32 (1990) 1301.

[10] J Goetz, B. Lipschultz, B. LaBombard et al, J Nucl. Mater., this conference.

[11] B L Welsh, H R Griem J C Moreno et al, Bull Amer Phys Soc 38(10) 1993, paper 3S20, pg 1957.

[12] J L Terry et al Rev Sci Instrum. to be published , 1994

[13] C Kurz, J A Snipes, J L Terry et al, Rev Sci Instrum. to be published , 1994.

[14] C Kurz, B Lipschultz, G M McCracken et al, J Nucl. Mater., this conference.

[15] R A Hulse, Nuclear Technology/Fusion, 3 (1983) 259.

[16] K Borass and G Janeschitz, Nuclear Fusion, to be published

[17] G. Janeschitz, S. Clement, N. Gottardi et al, Proc. 18th European Physical Conf.

on Controlled Fusion and Plasma Physics, Innsbruck Vol II (1992) 727.

[18] T W Petrie et al, J. Nucl. Mat. 196-198 (1992) 848.

[19] N. Hosogane et al, J. Nucl. Materials, 196-198 (1992) 750.

[20] L L Lao, H St John, R D Stambaugh et al, Nuclear Fusion 25(1985)1611

[21] I H Hutchinson Nuclear Fusion, (1994) to be published

[22] M. Greenwald, J. Terry, S. Wolfe, S. Ejima et al, Nucl. Fusion 28 (1988).

[23] M Graf et al Rev Sci Instrum. to be published.

[24] G M McCracken F Bombarda, B Labombard et al J Nucl. Mater. this conference

[25] K Lackner, R Chodura,M Kaufmann et al Plasma Phys Cont. Fus. 26 (1984) 105.

[26] P J Harbour, Nuclear Fusion 24 (1984) 1211

Figure Captions

Figure 1: Layout of the Alcator C-Mod vacuum vessel and first-wall hardware.

Figure 2: Location of the Langmuir probes in the divertor and SOL. The 'domed' probes are denoted with a 'D' beside the location number.

Figure 3: Two arrays of 4 bolometer detectors view the divertor region. The chords are labeled B1-B8. An additional array of UV/visible-sensitive diodes, UV1 - 16 is shown as well.

Figure 5: Radiated power in the divertor region (□) is plotted vs. $\bar{n}_e$. $P_{RAD,div}/P_{SOL}$, the fraction of the power flowing in the SOL which is radiated is plotted as well (○).

Figure 6: Scaling of the divertor density at probe OD-7 vs. $\bar{n}_e$. Two sets of data are shown; □ - 500 kA $\leq I_p \leq$ 700 kA, ○ - 700 kA $\leq I_p \leq$ 900 kA.

Figure 7: I_{SAT} for outer divertor probes OD-1 through OD-10 through a detachment

at 0.725 seconds. Locations of the probes are given in figure 2.

Figure 8: The effect of detachment on central and divertor parameters for the same shot as figure 7.

Figure 9: Illustration of localized detachment preceding a general divertor detachment at 0.67 sec. The peak in the I_{SAT} progressively moves up the divertor face. A corresponding movement of radiation due to the localized detachment is evident on the XUV array signals which view the same region of the outer divertor surface (see figure 3).

Figure 10: Density threshold for detachment vs. Input power. Data is shown for both ohmic (○) and RF-heated discharges (◆).

Figure 11: Neutral density at the divertor surface (◆) and in the SOL (●) before detachment.

Figure 12: C-III emissivity after detachment. The peak emission is 270 W/m^3 and is located above the x-point. Bolometer chord B1 indicates the same location.

Figure 13:Target temperature from probe 7 for different regimes of SOL transport. (△) 600 kA≤ I_p≤700 kA (experiment); (+) 800 kA≤ I_p≤900 kA, experiment; Fits from the two point model: solid line for the higher current, dashed line for the lower current.

Figure 14: Illustration of the localized detachment. The region of pressure gradient along a flux surface is shaded and labeled local detachment 'front'.

Table 1 Alcator C-Mod Parameters

Parameter	Design Value (achieved)
Toroidal Field	9 Tesla (5.4)
Plasma Current	3 MA (1.1)
Major radius	.67 m
Minor radius	.21 m
Kappa	1.8 (1.65)
P_{ICRF}	4 MW (1MW)

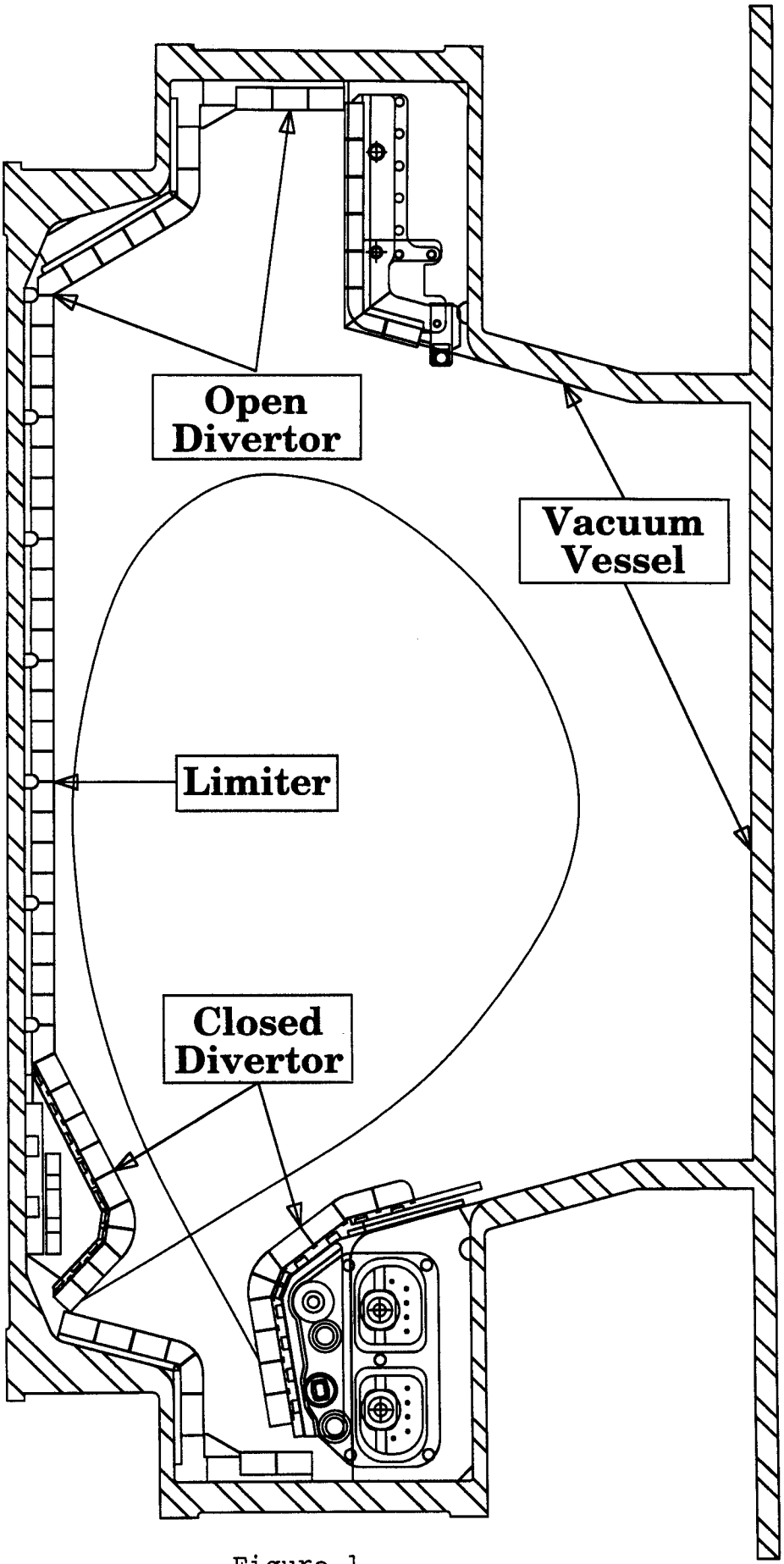

Figure 1

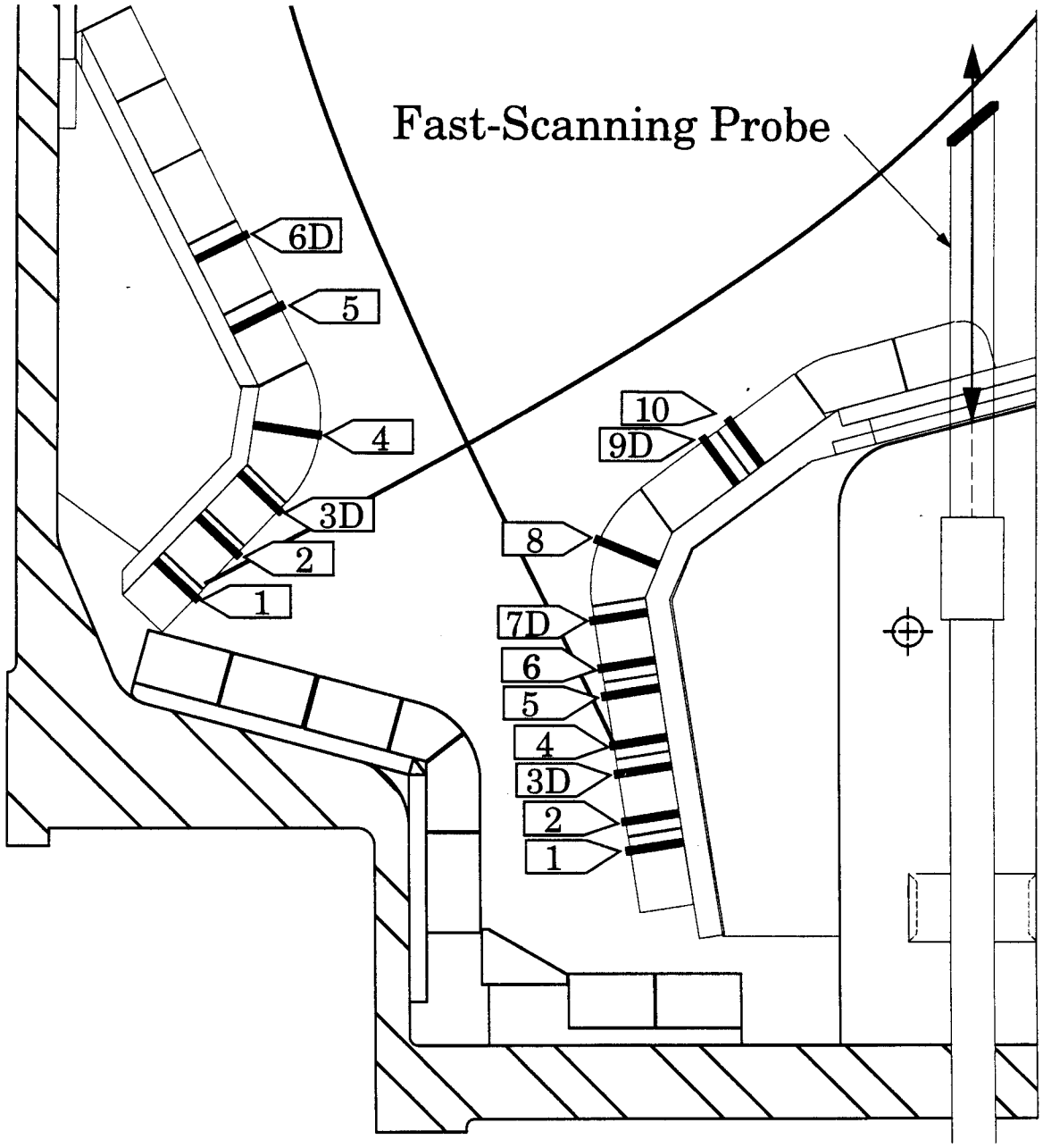

Figure 2

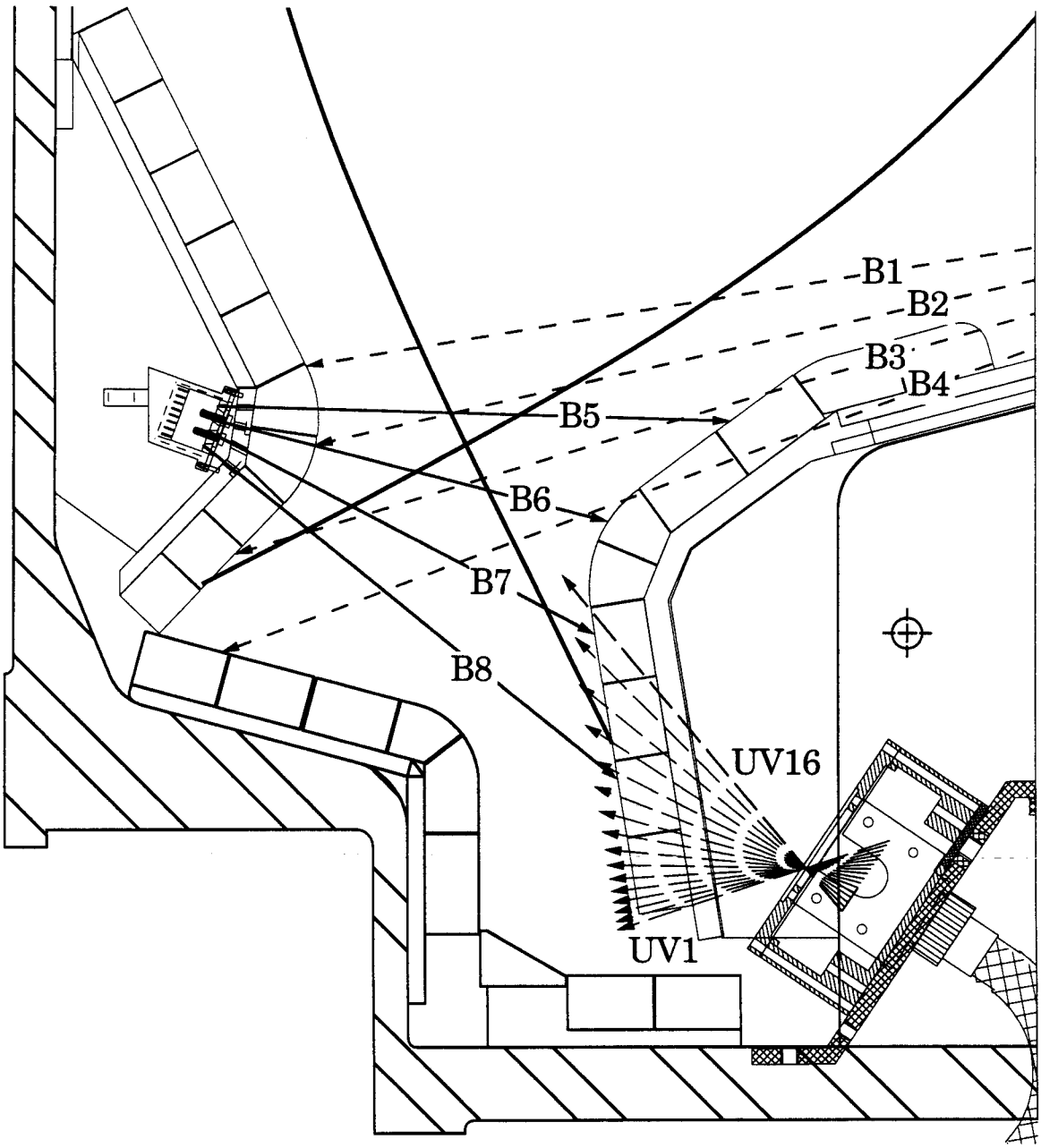

Figure 3

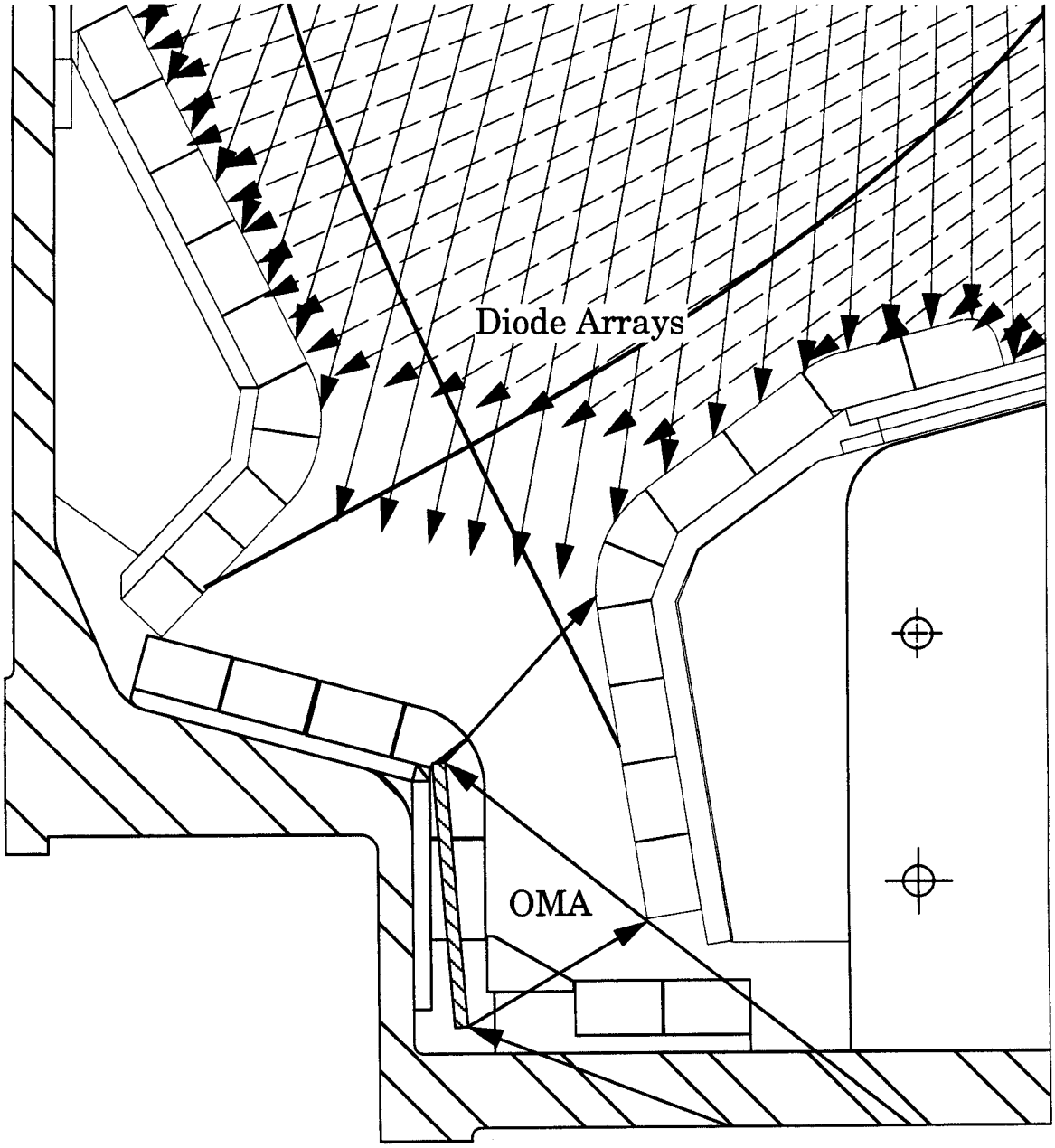

Figure 4

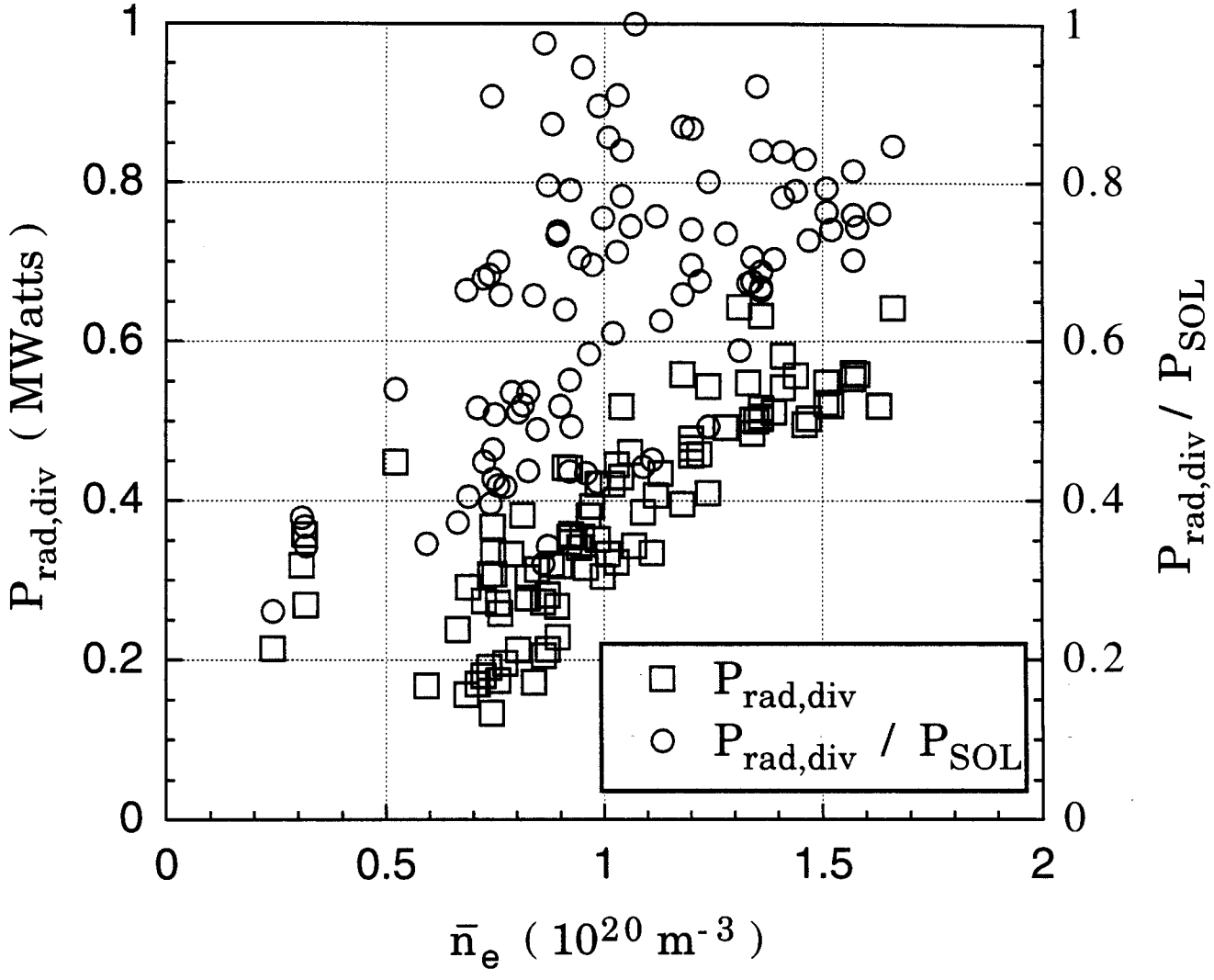
1
0.8
0.6
0.4
0.2
0
0
0.5
1
1.5
2
$P_{rad,div}$ (MWatts)
$P_{rad,div}$ / P_{SOL}
$\bar{n}_e$ (10^{20} m^{-3})
$P_{rad,div}$
$P_{rad,div}$ / P_{SOL}

Figure 5

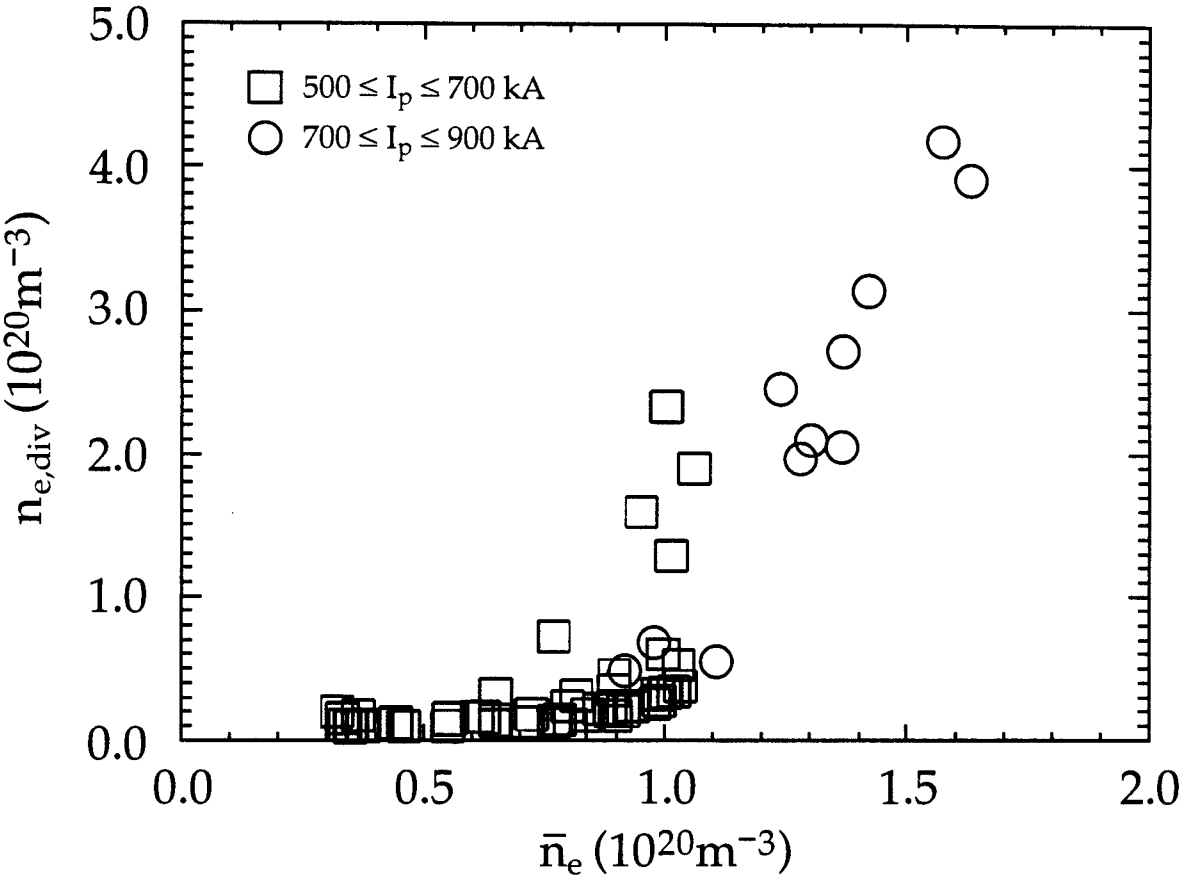
5.0
4.0
3.0
2.0
1.0
0.0
0.0
0.5
1.0
1.5
2.0
$n_{e,div}$ ($10^{20}m^{-3}$)
$\bar{n}_e$ ($10^{20}m^{-3}$)
$500 \leq I_p \leq 700$ kA
$700 \leq I_p \leq 900$ kA

Figure 6

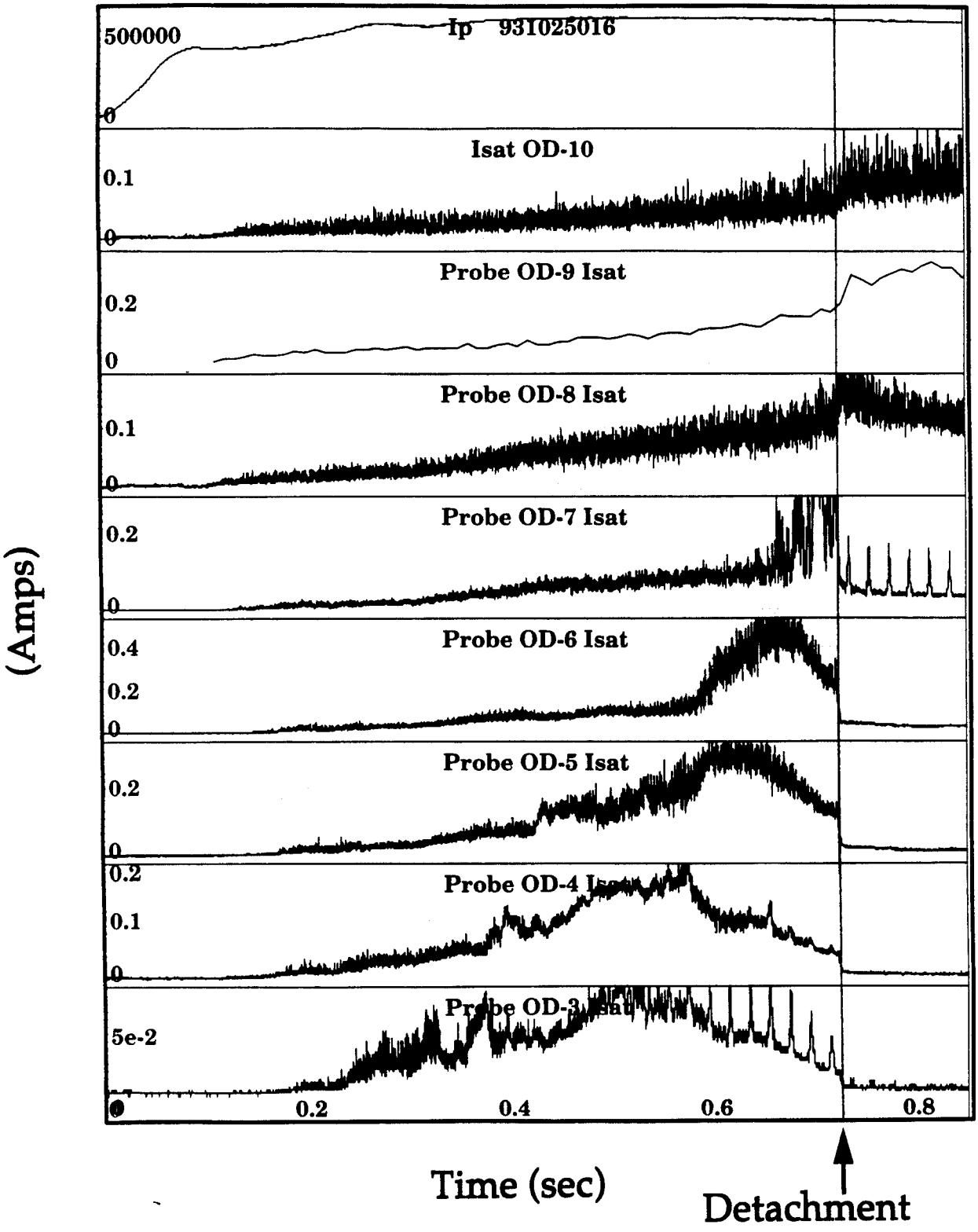
500000
Ip 931025016
0
Isat OD-10
0.1
0
Probe OD-9 Isat
0.2
0
Probe OD-8 Isat
0.1
0
Probe OD-7 Isat
0.2
0
Probe OD-6 Isat
0.4
0.2
0
Probe OD-5 Isat
0.2
0
0.2
Probe OD-4 Isat
0.1
0
Probe OD-3 Isat
5e-2
0
0.2
0.4
0.6
0.8
(Amps)
Time (sec)
Detachment

Figure 7

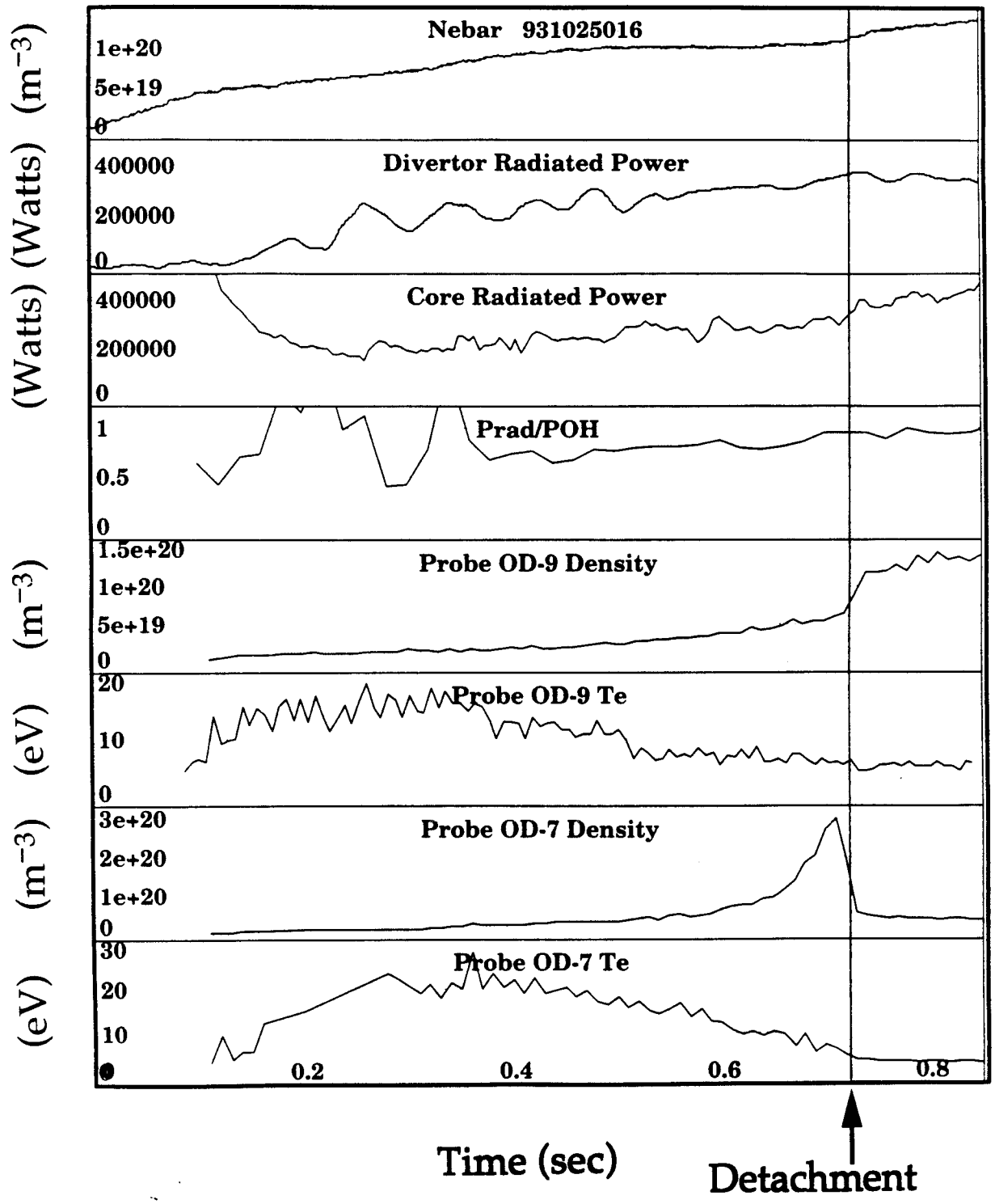
Nebar 931025016
1e+20
5e+19
0
(Watts) (Watts) (m^{-3})
400000
200000
0
Divertor Radiated Power
400000
200000
0
Core Radiated Power
1
0.5
0
Prad/POH
1.5e+20
1e+20
5e+19
0
(m^{-3}) (m^{-3})
Probe OD-9 Density
20
10
0
(eV) (eV)
Probe OD-9 Te
3e+20
2e+20
1e+20
0
(m^{-3}) (m^{-3})
Probe OD-7 Density
30
20
10
0
(eV) (eV)
Probe OD-7 Te
0.2
0.4
0.6
0.8
Time (sec)
Detachment

Figure 8

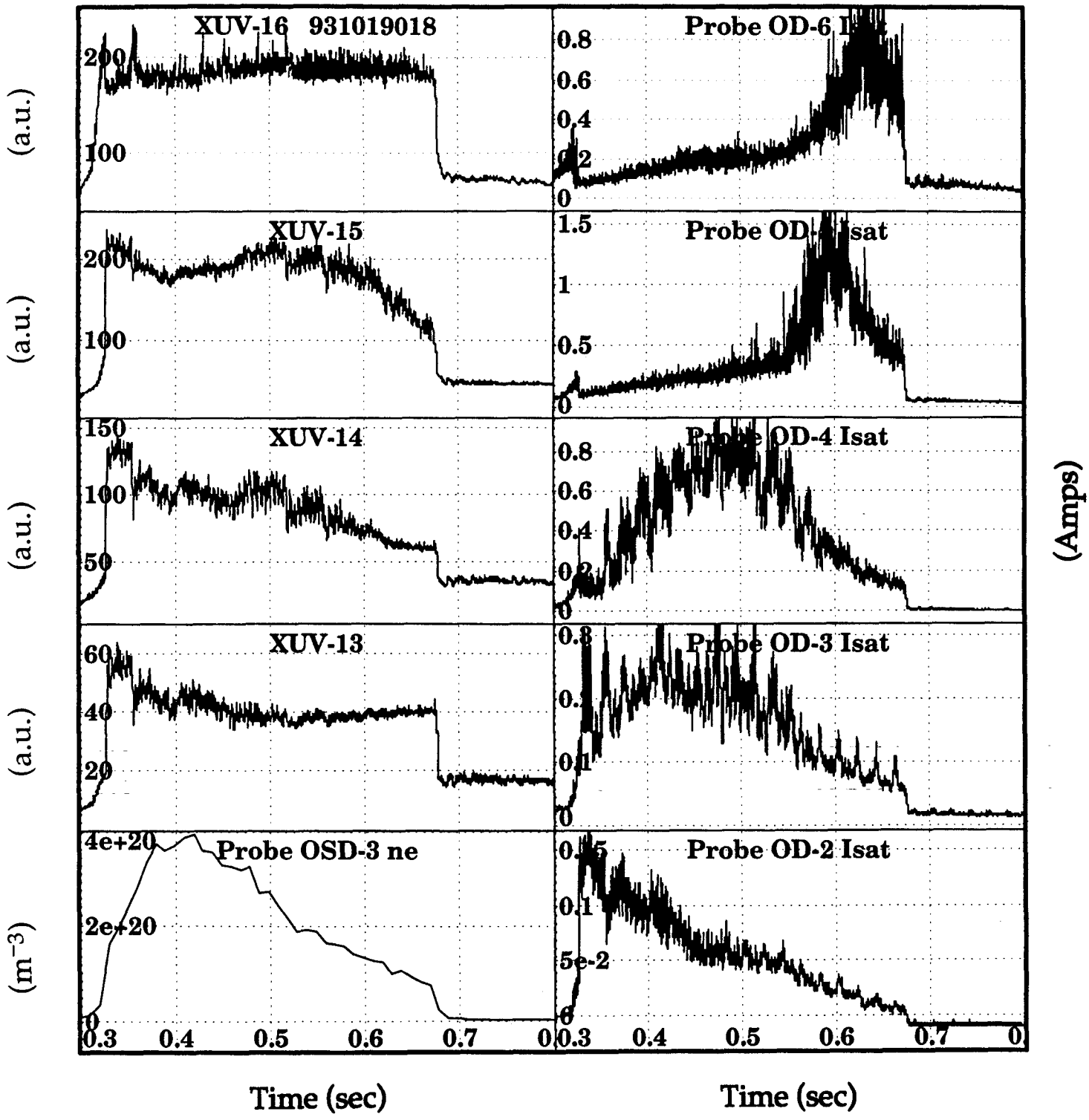
XUV-16 931019018
XUV-15
XUV-14
XUV-13
Probe OSD-3 ne
Probe OD-6 I
Probe OD-4 Isat
Probe OD-3 Isat
Probe OD-2 Isat
(a.u.)
(a.u.)
(a.u.)
(a.u.)
(m^{-3})
(Amps)
Time (sec)
Time (sec)

Figure 9

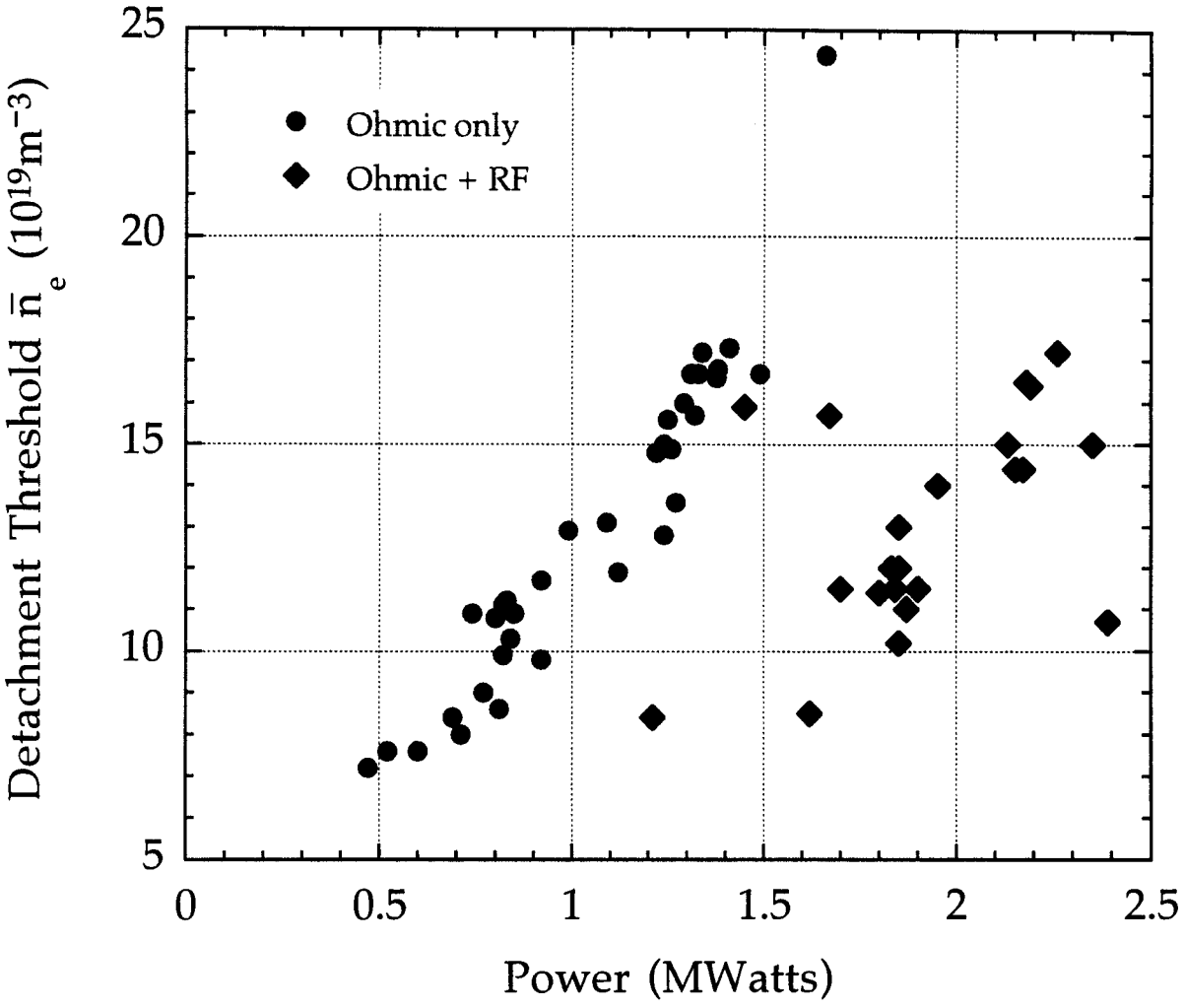
Ohmic only
Ohmic + RF
Detachment Threshold $\bar{n}_e$ ($10^{19}m^{-3}$)
Power (MWatts)
25
20
15
10
5
0
0.5
1
1.5
2
2.5

Figure 10

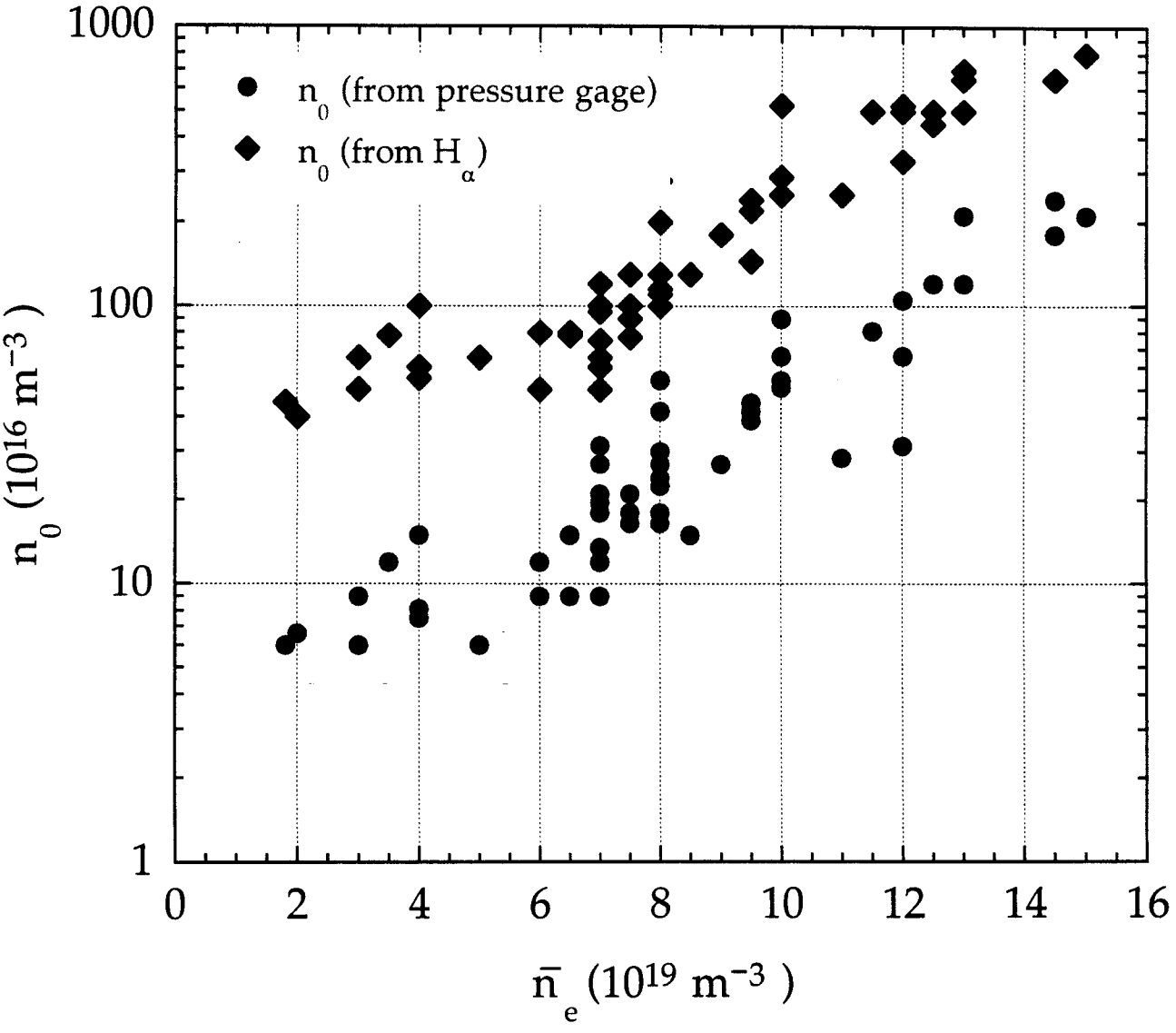
1000
100
10
1
0
2
4
6
8
10
12
14
16
n0 (from pressure gage)
n0 (from Hα)
n0 (10^16 m^-3)
n̄e (10^19 m^-3)

Figure 11

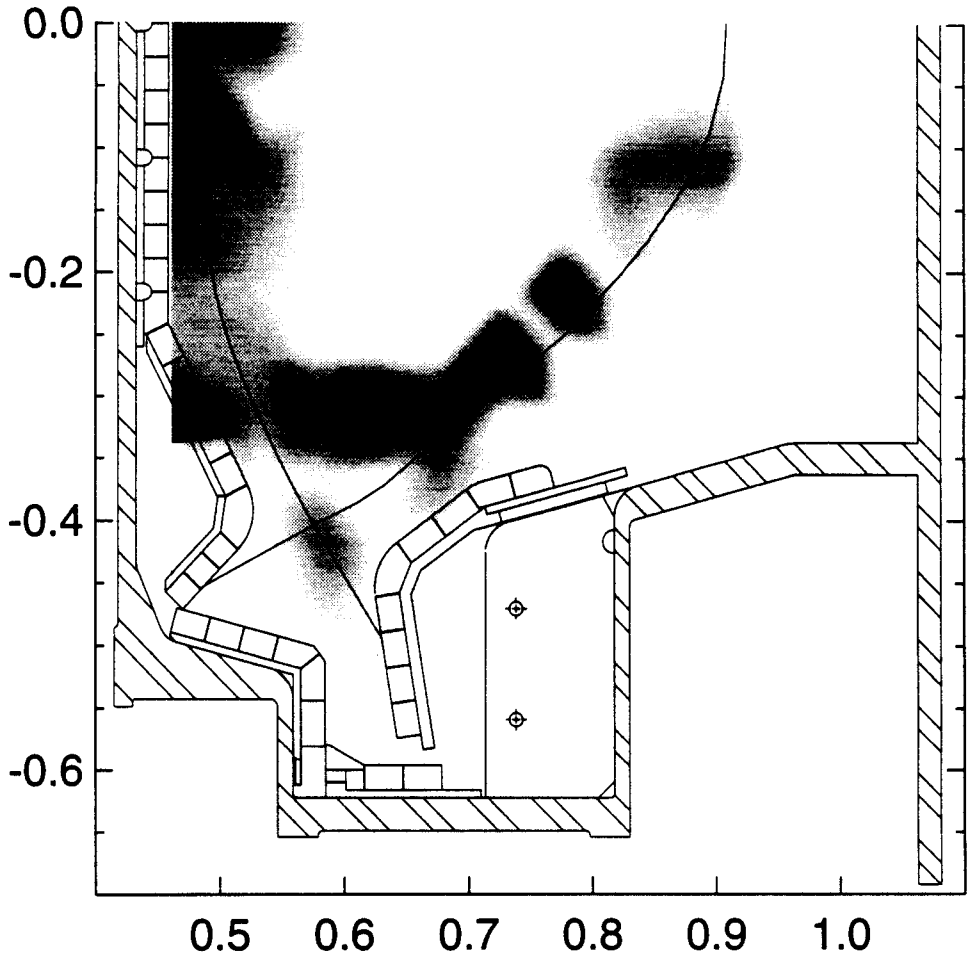

Figure 12

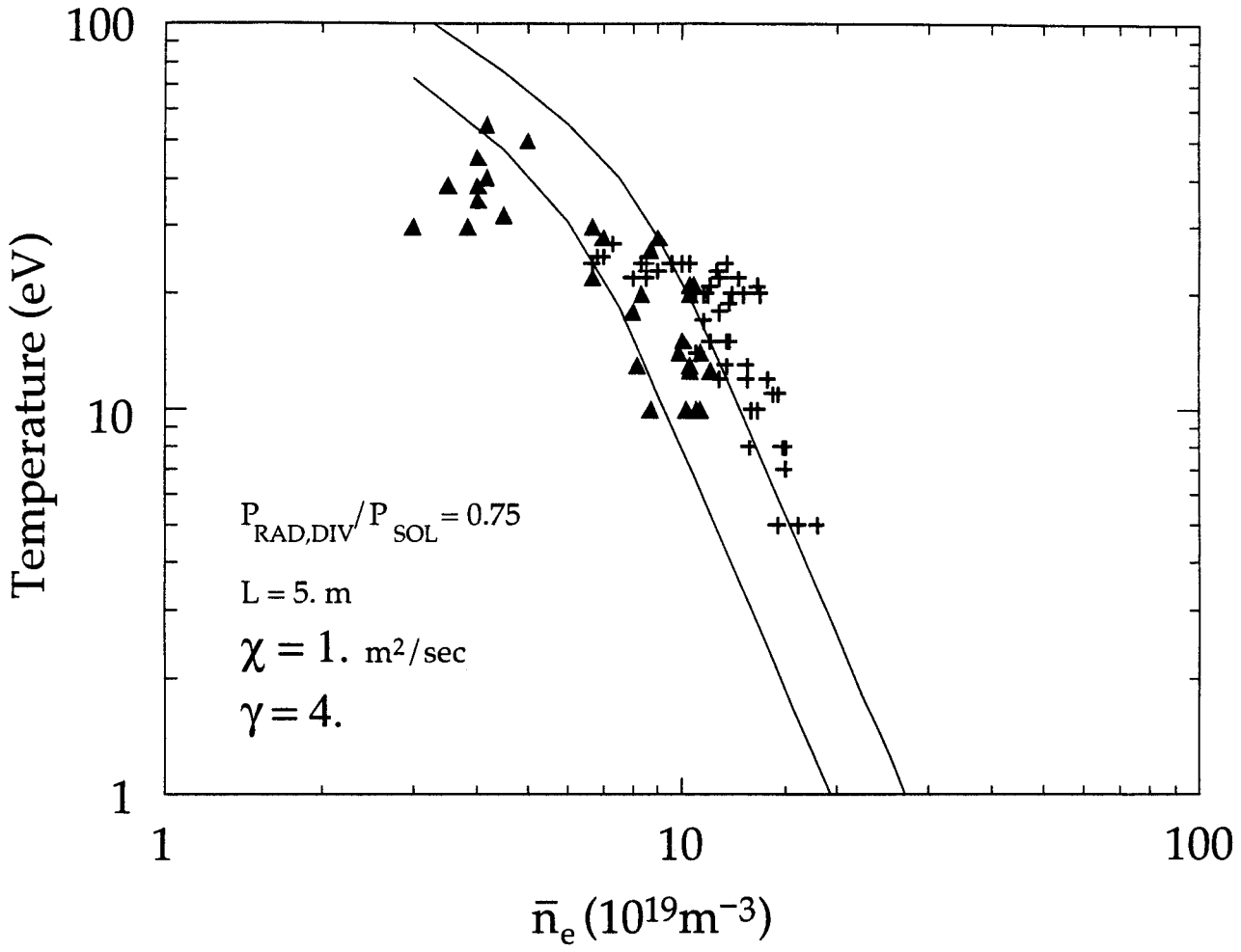
100
10
1
1
10
100
Temperature (eV)
$\bar{n}_e (10^{19} m^{-3})$
$P_{RAD,DIV}/P_{SOL} = 0.75$
L = 5. m
$\chi = 1.$ m²/sec
$\gamma = 4.$

Figure 13

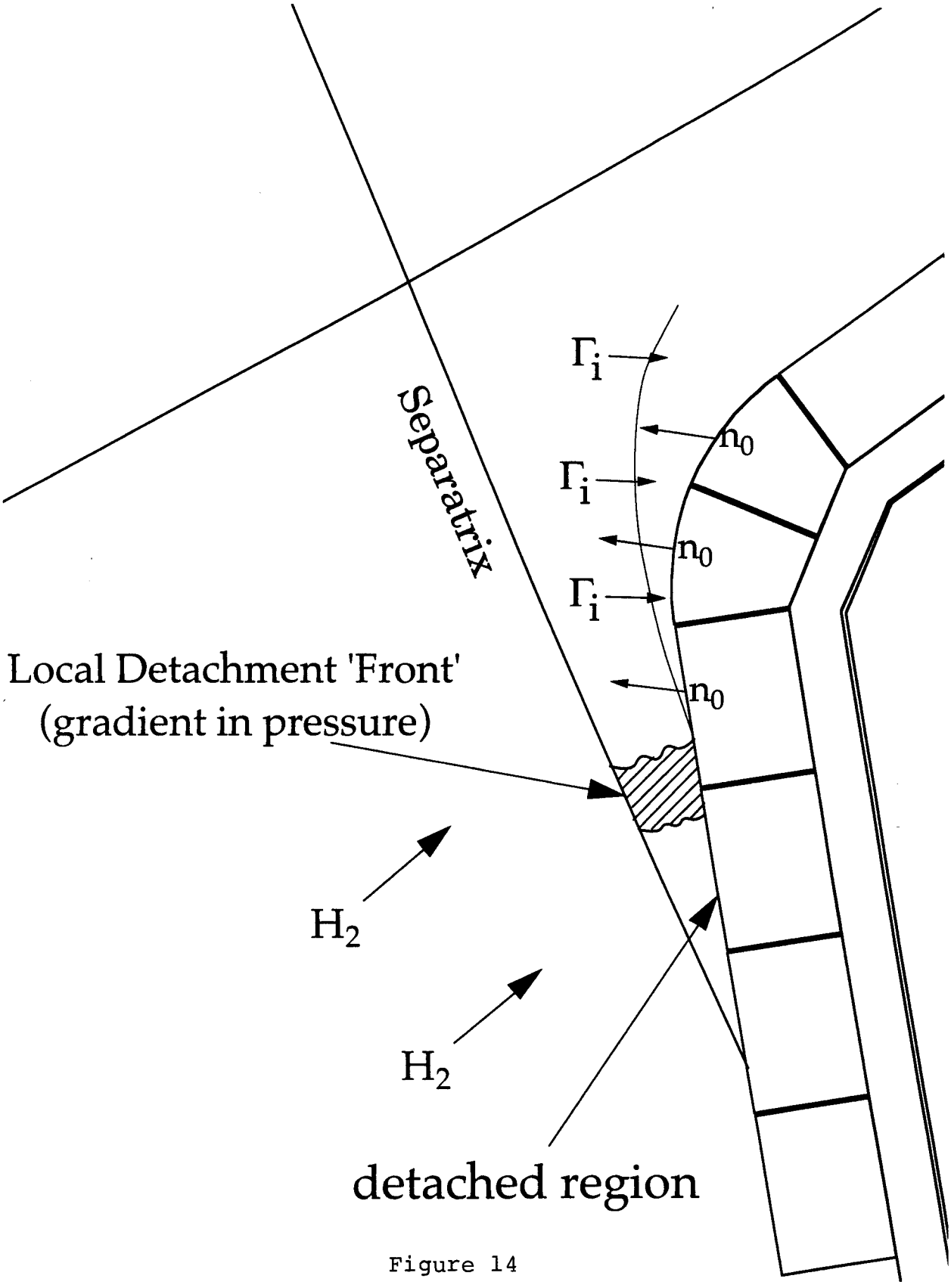
Separatrix
Γ_i
n_0
Γ_i
n_0
Γ_i
n_0
Local Detachment 'Front'
(gradient in pressure)
H_2
H_2
detached region

Figure 14